Modifying the β,γ Leaving-Group Bridging Oxygen Alters Nucleotide Incorporation Efficiency, Fidelity, and the Catalytic Mechanism of DNA Polymerase β[†]

Christopher A. Sucato,[‡] Thomas G. Upton,[‡] Boris A. Kashemirov,[‡] Vinod K. Batra,[§] Václav Martínek,[||,⊥] Yun Xiang,[‡] William A. Beard,[§] Lars C. Pedersen,[§] Samuel H. Wilson,[§] Charles E. McKenna,[‡] Jan Florián,[||,#] Arieh Warshel,[‡] and Myron F. Goodman*[,‡,△]

Departments of Biological Sciences and Chemistry, University of Southern California, Los Angeles, California 90089, Department of Chemistry, Loyola University, Chicago, Illinois 60626, Department of Biochemistry, Faculty of Science, and Institute of Physics, Charles University, Prague, Czech Republic, and Laboratory of Structural Biology, NIEHS, National Institutes of Health, DHHS, Research Triangle Park, North Carolina 27709

Received July 27, 2006; Revised Manuscript Received October 18, 2006

ABSTRACT: DNA polymerase catalysis and fidelity studies typically compare incorporation of "right" versus "wrong" nucleotide bases where the leaving group is pyrophosphate. Here we use dGTP analogues replacing the β,γ-bridging O with CH_2, CHF, CF_2, or CCl_2 to explore leaving-group effects on the nucleotidyl transfer mechanism and fidelity of DNA polymerase (pol) β. T·G mismatches occur with fidelities similar to dGTP with the exception of the CH_2 analogue, which is incorporated with 5-fold higher fidelity. All analogues are observed to bind opposite template C with K_ds between 1 and 4 μM, and structural evidence suggests that the analogues bind in essentially the native conformation, making them suitable substrates for probing linear free energy relationships (LFERs) in transient-kinetics experiments. Importantly, Brønsted correlations of $\log(k_{pol})$ versus leaving-group pK_a for both right and wrong base incorporation reveal similar sensitivities ($\beta_{lg} \approx -0.8$) followed by departures from linearity, suggesting that a chemical step rather than enzyme conformational change is rate-limiting for either process. The location of the breaks relative to pK_as of CF_2, O, and the sterically bulky CCl_2-bridging compounds suggests a modification-induced change in the mechanism by stabilization of leaving-group elimination. The results are addressed theoretically in terms of the energetics of successive primer 3′-O addition (bond forming) and pyrophosphate analogue elimination (bond breaking) reaction energy barriers.

DNA replication and repair pathways involve balancing an essential need for high-fidelity synthesis to ensure accurate genome duplication, with specialized needs for much lower fidelity synthesis to copy replication-blocking DNA lesions, and to provide beneficial mutations crucial for immunodiversity and evolution. To regulate when and where high- and low-fidelity polymerases come into play requires complex interactions involving polymerases and a wide variety of protein cofactors (*1*).

These complexities not withstanding, the fidelity of DNA synthesis is determined for the most part by the structural and catalytic properties of the polymerase interacting with its template, primer, and dNTP substrates, where the nature of the constituent purine or pyrimidine base should dominate in base pair recognition. However, the contribution of leaving-group effects to the catalytic process for correct and incorrect DNA synthesis, particularly in terms of the crucial but so-far obscure transition states involved, is unknown. Here we address an unexplored aspect of this question by assessing the effects of modifying the dNTP triphosphate β,γ-bridging oxygen on (1) the polymerase−substrate ternary structures, (2) the catalytic efficiency, and (3) the fidelity of human DNA polymerase (pol)[1] β. Pol β has been used extensively as a model system to investigate fidelity (*2*, *3*) based on its central role in DNA repair (*4*), buttressed by the availability of numerous crystal structures of various liganded states (*5*−*7*).

A mechanistic understanding of fidelity for any polymerase would require detailed knowledge of the probabilities of observing the structures along trajectories of the system corresponding to reaction coordinates reflecting correct and incorrect base pairing reactions. These probabilities are typically represented as free energy diagrams. Focusing on the chemical transformations (Figure 1), binding of dNTP substrate to the polymerase active site together with template and primer is believed to be followed by nucleophilic attack of the target DNA 3′-oxygen (activated by deprotonation)

[†] This work was supported by the Intramural Research Program of the NIH, National Institute of Environmental Health Sciences, and by National Institutes of Health Grants 1U19CA10501 and R37GM21422.

* To whom correspondence should be addressed. Telephone: (213) 740-5190. Fax: (213) 740-8631. E-mail: mgoodman@usc.edu.

[‡] Department of Chemistry, University of Southern California.

[§] Laboratory of Structural Biology, NIEHS.

[||] Department of Chemistry, Loyola University.

[⊥] Department of Biochemistry, Charles University.

[#] Institute of Physics, Charles University.

[△] Department of Biological Sciences, University of Southern California.

[1] Abbreviations: pol, DNA polymerase; LFER, linear free energy relationship; $O_{\alpha\beta}$, α,β-bridging triphosphate oxygen; $O_{\beta\gamma}$, β,γ-bridging triphosphate oxygen; lg, leaving group; MD, molecular dynamics; FEP, free energy perturbation; EVB, empirical valence bond; TS, transition state.

10.1021/bi061517b CCC: $37.00
Published on Web 12/15/2006

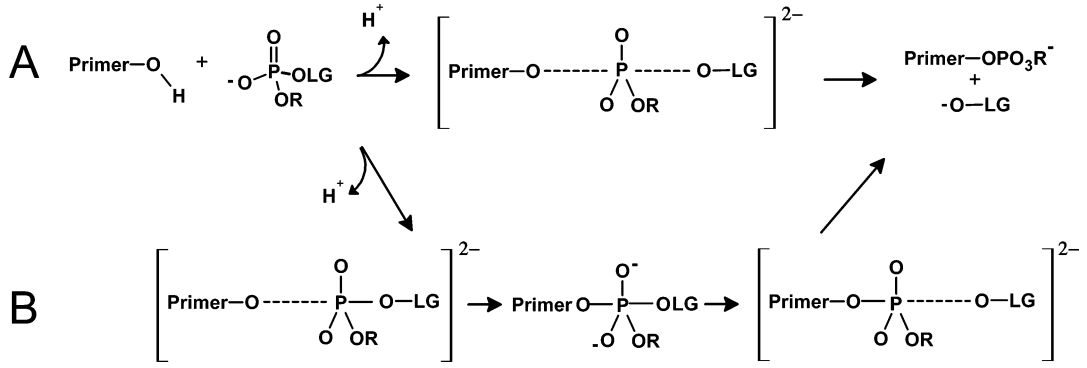

FIGURE 1: Chemical steps involved in nucleotidyl transfer. Deprotonation of the primer 3′-hydroxyl is followed by nucleophilic attack on the P_α of the dNTP. Cleavage of the $P_\alpha-O_{\alpha\beta}$ bond results in elimination of the leaving group (LG, above). Whether the pol β-catalyzed transition state occurs via a (A) concerted or (B) stepwise mechanism is not known. In the concerted model a significant amount of bond forming and bond breaking about P_α occurs simultaneously through a single activation barrier. In the stepwise model a short-lived pentacovalent intermediate exists between separate bond-forming and -breaking steps, resulting in two separate activation barriers. The models are extreme cases; the actual reaction coordinate may adopt a trajectory intermediate between the two.

on P_α of the triphosphate moiety (addition step), followed by departure of pyrophosphate (elimination step) (*8*). A key point is that, in the absence of marked steric effects induced by leaving-group modification, the nucleotide incorporation reaction rate constants for both right and wrong substrates should correlate with the acidity of the leaving-group moiety, depending on which step (if either) is rate-limiting. In a rate-limiting addition step, extra negative charge is transferred onto P_α, and thus a modest sensitivity to polarity changes in the remote β,γ-bridging group might result. However, a larger effect would be expected if elimination were rate-limiting, because in this case the stability of the anionic leaving group should be substantially sensitive to such changes.

Kinetic experiments designed to introduce small perturbations to the polymerase complex could help to reveal information about free energy changes at well-defined positions along the reaction coordinate. Here we describe a strategy for probing the nucleotidyl transfer mechanism by constructing a linear free energy relationship (LFER) correlating the catalytic rate constant, k_{pol}, with leaving-group solution pK_as for a series of dNTP analogues modified at the β,γ-bridging position. LFERs between equilibrium and kinetic substituent effects are well-known tools for deciphering reaction mechanisms in solution (*9*) and in enzymatic reactions (*10*, *11*), and Brønsted correlations between leaving-group pK_a and catalytic rate constants have been reported (*12*−*14*).

The transient-state single-turnover assays reported here reveal a linear Brønsted correlation, with $\beta_{lg} \approx -0.8$ in the leaving-group pK_{a4} range 9−11, consistent with β_{lg}s reported for other enzymatic P−O bond cleavages (*12*, *13*). At lower pK_a, however, we find virtually no sensitivity ($\beta_{lg} \approx 0$) for either correct or mismatch incorporation. For correct pairing, all of the analogues studied here bind in pol β ternary complexes with K_ds close to that of native dGTP (1−4 μM), and X-ray crystallographic data for the CF_2- and CH_2-bridging analogues show virtually no deviation from the native conformation of the triphosphate moiety. Taken together, these data suggest a leaving-group-induced change in the rate-liming step due to stabilization of pyrophosphate (or analogue) elimination. A steric-repulsion explanation for the catalytic insensitivity, observed with CF_2, can be ruled out, as the bulkier CCl_2-containing analogue conforms to LFER behavior. We explore the significance of these results on pol β catalysis and fidelity, aided in part by molecular dynamics simulations in which free energies are explicitly computed. By evaluating free energy surfaces associated with leaving-group-modified substrates, the simulations are intended to lend additional insight into the experimental results.

MATERIALS AND METHODS

Materials. High purity solution dGTP and T4 polynucleotide kinase (Optikinase) were purchased from Amersham Biosciences. DNA synthesis reagents and protected deoxyribonucleoside phosphoramidites were purchased from Applied Biosystems. Radiolabeled [γ-^{32}P]ATP was purchased from MP Biomedicals. Buffer components and all other chemicals were purchased from Fisher Scientific, Sigma, or VWR. The β,γ-CH_2, CHF, CF_2, and CCl_2 analogues of dGTP were prepared from dGMP (Sigma) morpholidate (*15*) and the corresponding methylenebisphosphonic acid, purified by two-stage preparative HPLC (>99%), and characterized by ^{1}H, ^{31}P, ^{19}F NMR and UV−visible spectra, analytical HPLC (Varian PureGel R00087E1PE 7 μM 500A SAX), and negative ion FAB or MALDI HRMS. Synthetic and analytical details for the analogues will be presented elsewhere. The CF_2 analogue was previously prepared by a different method (*16*).

Purification and Quantitation of Pol β. Human pol β was purified as described previously (*17*). Enzyme concentrations were determined by Coomassie dye binding using purified pol β as the standard. The concentration of purified pol β was determined by total amino acid analysis.

Crystallization of the Pol β Substrate Complexes and Structure Determination. Human DNA polymerase β was overexpressed in *Escherichia coli* and purified. The DNA substrate consisted of a 16-mer template, a complementary 9-mer primer strand, and a 5-mer downstream oligonucleotide. The annealed oligonucleotides create a two-nucleotide gapped DNA substrate. The sequence of the downstream oligonucleotide was GTC GG and the 5′-terminus was phosphorylated. The template and primer sequences were CCG ACC GCG CAT CAG C and GCT GAT GCG, respectively. Oligonucleotides were dissolved in 20 mM $MgCl_2$ and 100 mM Tris-HCl, pH 7.5. The template, primer,

and downstream oligonucleotides were mixed in a 1:1:1 ratio and annealed using a PCR thermocycler by heating for 10 min at 90 °C and cooling to 4 °C (1 °C min^{-1}), resulting in a 1 mM mixture of gapped duplex DNA. This solution was then mixed with an equal volume of pol β (15 mg/mL in 20 mM Bis-Tris, pH 7.0) at 4 °C; the mixture was warmed to 35 °C and gradually cooled to 4 °C. A 4-fold excess of ddCTP was added to the two-nucleotide gapped complex to obtain a one-nucleotide gap complex with a dideoxy-terminated primer terminus.

Pol β−DNA complexes were crystallized by sitting-drop vapor diffusion. The crystallization buffer for the binary one-nucleotide gap consisted of 16% PEG-3350, 350 mM sodium acetate, and 50 mM imidazole, pH 7.5. Drops were incubated at 18 °C and streak seeded after 1 day. Crystals grew in approximately ∼2−4 days after seeding. The binary complex crystals were soaked in artificial mother liquor containing 200 mM $MgCl_2$, 90 mM sodium acetate, 4−6 mM dGTP-($\beta-\gamma$ CF_2) or dGTP($\beta-\gamma$ CH_2), 20% PEG-3350, and 12% ethylene glycol.

Data were collected at 100 K on a CCD detector system mounted on a MicroMax-007HF (Rigaku Corp.) rotating anode generator. Data were integrated and reduced with HKL2000 software (*18*). Ternary substrate complex structures were determined by molecular replacement with a previously determined structure of pol β complexed with one-nucleotide-gapped DNA and a complementary incoming ddCTP (PDB accession number 1BPY) (*7*). The parameters and topology files for the nucleotide analogues were prepared using the program XPOL2D (*19*). The crystal structures have similar lattices and are sufficiently isomorphous to determine the molecular replacement model using CNS and manual model building using O (*20*). The crystallographic statistics for the ternary complex structures with dGTP($\beta-\gamma$ CF_2) and dGTP($\beta-\gamma$ CH_2) are tabulated in Table 1. The coordinates and structure factors have been deposited in the RCSB protein databank with accession codes 2ISO and 2ISP, respectively.

DNA Synthesis and Purification. Primer (TAT TAC CGC GCT GAT GCG C), template (GCG TTG TTC CGA CMG CGC ATC AGC GCG GTA ATA; M = C, T), and 5′-end-phosphorylated downstream (GTC GGA ACA ACG C) oligomers were synthesized on a solid-phase DNA synthesizer (Applied Biosystems Model 3400), cleaved from the polystyrene support and deprotected with 30% (v/v) ammonium hydroxide (55 °C, ∼12 h), and purified by denaturing polyacrylamide gel electrophoresis. The product bands were located by UV shadowing over a fluorescent TLC plate, excised from the gel, and crushed, and the DNA was extracted by elution into STE buffer. Volumes were reduced by vacuum, and salt was removed by dialysis into distilled water. DNA concentrations were determined by absorbance at 260 nm using a molar absorption coefficient calculated from the sum of the constituent nucleotides. Oligomers were stored in filtered, distilled water at −20 °C.

DNA Radiolabeling and Annealing. Primer DNA (1 molar equiv) was 5′-end labeled using T4 polynucleotide kinase (0.4 unit/μL) and [γ-^{32}P]ATP (∼0.7 molar equiv) using the supplied buffer. The kinase was inactivated after 30 min by heating at 90 °C for 10 min, and the reaction mixture was used for annealing without further purification. Annealing was carried out by mixing primer, template (1.2 molar equiv), and downstream (1.5 molar equiv) oligomers, heating to 90 °C, and then cooling slowly to room temperature.

Table 1: Crystallographic Data Collection and Refinement Statistics

complex	dGTP($\beta-\gamma$ CF_2)	dGTP($\beta-\gamma$ CH_2)
Data Collection		
space group	$P2_1$	$P2_1$
a (Å)	50.7	50.7
b (Å)	80.5	80.4
c (Å)	55.4	55.5
β (deg)	108.0	107.9
d_{min} (Å)	2.10	2.20
R_{merge} (%)[a]	11.7 (43.6)[b]	13.4 (58.5)
completeness (%)	99.9 (100)	97.7 (96.4)
I/σ_I	8.7 (3.1)	7.5 (2.5)
no. of observed reflections	90491	79136
no. of unique reflections	24642 (2453)	21102 (2063)
Refinement Statistics		
rms deviations		
bond lengths (Å)	0.005	0.005
bond angles (deg)	1.12	1.09
R_{work} (%)[c]	20.1	20.0
R_{free} (%)[d]	26.0	26.1
average *B* factor (Å^2)		
protein	26.3	26.2
DNA	38.3	39.0
dGDP(CH_2)P	18.4	14.6
Ramachandran analysis (%)[e]		
favored	98.5	98.8
allowed	100	100

[a] $R_{merge} = 100(\sum_h\sum_i|I_{h,i} - I_h|/\sum_h\sum_i I_{h,i})$, where I_h is the mean intensity of symmetry-related reflections $I_{h,i}$. [b] Numbers in parentheses refer to the highest resolution shell of data (10%). [c] $R_{work} = 100(\sum||F_o| - |F_c||/\sum|F_o|)$. [d] R_{free} for a 5% subset of reflections withheld from refinement. [e] As determined by MolProbity (*51*).

Single-Turnover Gap-Filling Assays. Single-nucleotide gapped DNA (template C or T) was preincubated for 2 min at 37 °C with pol β in assay buffer [50 mM Tris-HCl, 20 mM KCl, 20 mM NaCl, 10 mM $MgCl_2$, 1 mM DTT, 6% (v/v) glycerol, pH 7.9 at 23 °C] and then mixed with a solution of substrate (dGTP or analogue in assay buffer at 37 °C). Concentrations after mixing were 300 nM pol β, 50 nM DNA, and 0.5−20 μM substrate (C·G incorporation) or 50−1500 μM substrate (T·G incorporation). The reaction mixture was quenched by ∼3-fold dilution with 500 mM EDTA. Reaction time ranges were 0.09−0.5 s (C·G) and 0.5−100 s (T·G). Reaction times under 20 s were carried out with a rapid-mixing chemical quench apparatus (KinTek Model RQF-3); otherwise, mixing was done manually with a micropipet. The radiolabeled 19-mer primer and 20-mer product were separated by denaturing polyacrylamide gel electrophoresis [39 × 33 × 0.035 cm, 20% (w/v) polyacrylamide, 8 M urea gels run at 55−60 W, 3−4 h]. The percentage of primer extended was measured by exposure of the dehydrated gel to a storage phosphor screen (Bio-Rad no. 170-7841) followed by detection of phosphorescence emission on an imaging system (Molecular Dynamics STORM 860).

Data Analysis. Kinetic assays were performed under single-turnover conditions (E ≫ S) where the time evolution of product formation fits a single exponential: $[P]_t = [P]_{final}(1 - \exp[-k_{obs}t])$, where P is the extended primer product and k_{obs} is the observed catalytic rate constant. The observed rate constants were plotted against the substrate concentrations, and the data were fit to the hyperbolic equation: $k_{obs} = k_{pol}[S]/([S] + K_d)$, where S is dNTP substrate (dGTP or analogue), k_{pol} is an overall rate constant for the slowest

Table 2: pK_as for Conjugate Acids of Pyrophosphate or Substituted Bisphosphonates[a]

−X−	pK_{a4}	−X−	pK_{a4}
$-CF_2-$	7.63	$-CCl_2-$	9.78
−O−	8.91	$-CH_2-$	10.7
−CHF−	9.44		

[a] Literature values (*21*−*24*) were measured at 25 °C and 0.1 M ionic strength, except for monofluoro- and dichloromethylenebisphosphonic acid (0.15 and 0.0 M, respectively); reported error ranged from 0.01 to 0.1. Those conditions closely matched our buffer solutions and were used as reference pK_as in the Brønsted equation (eq 1). The other pK_as did not show a reliable correlation with electron-withdrawing ability of the bridging group and were not considered.

nucleotide insertion step(s), and K_d is the dissociation constant for substrate binding. The kinetic data were fit to the Brønsted equation (eq 1) using the pK_a values (*21*−*24*) shown in Table 2. Three replicates were performed for each substrate/template base combination, and the best-fit values for k_{pol} and K_d are reported as the mean ± standard error.

Theoretical Analysis. The behavior of the LFER in pol β and in solution was determined using full EVB simulations to model the effect of leaving-group modification. Simplified calculations were also performed to analyze the LFER for hydrolysis of the nucleotide analogues in solution. The empirical valence bond/free energy perturbation (EVB/FEP) calculations (*25*) of the two reaction steps in aqueous solution and enzyme active site were carried out for trajectories generated by the all-atom molecular dynamics (MD) simulations using the Amber95 force field (*26*) and TIP3P model of water implemented in the program Q (*27*). The detailed description of these calculations and of the force field used for the substrates and Mg^{2+} is presented in the Supporting Information.

RESULTS

Leaving-Group pK_a Is Perturbed by $O_{\beta\gamma}$ Replacement. Single-turnover kinetic assays are used to measure pol β-catalyzed incorporation of a series of dGTP analogues into single-nucleotide gapped DNA (Figure 2). In order to characterize the energetics of the chemical steps involved in nucleotidyl transfer, we have probed the catalytic sensitivity to CH_2, CHF, CF_2, and CCl_2 replacement of the β,γ-bridging oxygen ($O_{\beta\gamma}$) of the dGTP substrate (**1**−**4**, Figure 2C). Nucleotidyl transfer from these compounds results in formation of the corresponding bisphosphonate, or pyrophosphate in the case of native dGTP (**5**−**8**, Figure 2C). pK_a values of the corresponding bisphosphonic acids at various temperatures and ionic strengths have been reported in the literature. Table 2 presents reported pK_{a4} values under conditions that closely resemble our kinetic assays. The trend, in order of decreasing acidity (CF_2 > O > CHF > CCl_2 > CH_2), correlates roughly with the presence of electronegative atoms on the β,γ-bridging group.

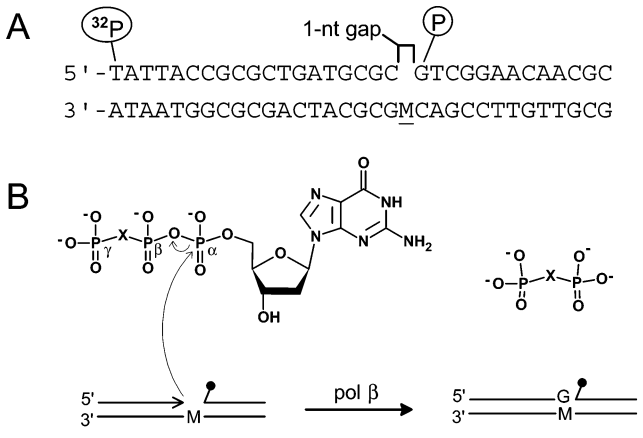

C

X	Nucleoside-Phosphate	Leaving-Group
O	dGTP	pyrophosphate
CH_2	**1** dGTP(β–γCH_2)	**5** methylenebisphosphonate
CHF	**2** dGTP(β–γCHF)	**6** monofluoromethylenebisphosphonate
CF_2	**3** dGTP(β–γCF_2)	**7** difluoromethylenebisphosphonate
CCl_2	**4** dGTP(β–γCCl_2)	**8** dichloromethylenebisphosphonate

FIGURE 2: Components of the single-turnover transient-kinetic assays of pol β-catalyzed incorporation of a series of dGTP analogues into single-nucleotide gapped DNA. (A) Primer/template/downstream oligomer DNA sequences. The template base (M, above) is C or T. The downstream oligomer is 5′-phosphorylated to induce optimal pol β binding (*6*). The local DNA sequence matches the local sequence used to obtain crystal structures with the analogues. (B) Structure of the dGTP substrate analogues and the leaving groups, where X represents the modified β,γ-bridging group. (C) Bridging groups studied here are shown in the table, with the nomenclature used in the text.

The origin of polar substituent effects on pK_a in the condensed phase has been attributed to contributions from through-space (field) and through-bond (inductive) effects, although controversy exists as to the relative magnitude of the latter (*28*, *29*). In any case, a lowered pK_a of the leaving group translates to stabilization of the negative charge developing on the α,β-bridging oxygen ($O_{\alpha\beta}$) during bond breaking. It follows from both Marcus theory in the condensed phase (*30*, *31*) and a more general adiabatic

Table 3: Kinetic and Thermodynamic Parameters for Pol β-Catalyzed Gap-Filling Assays[a]

M−N	−X−	k_{pol} (s^{-1})	K_d (μM)	k_{pol}/K_d (s^{-1} M^{-1})	f_{ins}
C−G	$-CF_2-$	21.9 ± 0.9	2.9 ± 0.34	$(7.5 \pm 0.9) \times 10^6$	
C−G	−O−	13.7 ± 1.3	1.3 ± 0.20	$(10.7 \pm 1.9) \times 10^6$	
C−G	−CHF−	16.6 ± 0.6	3.5 ± 0.63	$(4.8 \pm 0.9) \times 10^6$	
C−G	$-CCl_2-$	8.4 ± 1.0	3.7 ± 1.30	$(2.3 \pm 0.9) \times 10^6$	
C−G	$-CH_2-$	1.5 ± 0.2	0.75 ± 0.04	$(2.1 \pm 0.2) \times 10^6$	
T−G	$-CF_2-$	0.76 ± 0.01	380 ± 50	$(2.0 \pm 0.3) \times 10^3$	$(2.7 \pm 0.5) \times 10^{-4}$
T−G	−O−	1.34 ± 0.10	200 ± 7	$(6.6 \pm 0.5) \times 10^3$	$(6.2 \pm 1.2) \times 10^{-4}$
T−G	−CHF−	0.93 ± 0.06	270 ± 130	$(3.4 \pm 1.6) \times 10^3$	$(7.1 \pm 3.6) \times 10^{-4}$
T−G	$-CH_2-$	0.11 ± 0.01	430 ± 90	$(0.2 \pm 0.1) \times 10^3$	$(1.2 \pm 0.3) \times 10^{-4}$

[a] Assays were conducted under single-turnover conditions (see Materials and Methods). M−N is the template-incoming base pair and −X− is the β,γ-bridging group. Values of k_{pol} and K_d are reported as the mean ± standard deviation of three replicates, and error in the efficiencies (k_{pol}/K_d) and misinsertion frequency, f_{ins} (eq 2), was calculated according to the standard rules for error propagation. The Brønsted correlations of log(k_{pol}) versus p$K_{a,lg}$ are plotted in Figure 5, and the substituent effect on fidelity is depicted in Figure 8.

treatment (*11*) that stabilization of the products should also lead to stabilization of the preceding activation barrier according to a LFER. The so-called Brønsted relationship (eq 1) is one such LFER and can be derived in an essentially rigorous way using the modified Marcus relation (*10*, *11*) (Supporting Information, Figure 1S and eq 2S).

The LFER can be extended to a multistep reaction and used to analyze the corresponding mechanism (*32*) if the dominant effect of the modifications is at one well-defined position on the reaction coordinate (e.g., a bond-making or bond-breaking step). The trend observed in a Brønsted plot reflects the changes in the rate-limiting barriers caused by the given modification.

$O_{\beta\gamma}$ Replacement Does Not Affect the Conformation of Bound Substrate. Although the intended effect of $O_{\beta\gamma}$ replacement is on the negative charge developing on $O_{\alpha\beta}$, we must also consider the possibility of additional electrostatic and steric effects that may perturb other parts of the system. The effects of fluoromethylene replacement of the bridging oxygen in a phosphate ester or anhydride have been studied in detail in other systems (*33*), as this modification is widely recognized (*34*, *35*) to confer inertness to hydrolytic cleavage. The van der Waals radii of the fluoromethylene groups are estimated to be ~2-fold larger than that of oxygen, methylene being the best steric approximation (*36*). Despite these differences, phosphate mimics bearing fluoromethylene groups are reported to bind effectively in a number of enzyme active sites (ref *33* and references cited therein).

The structure of the pol β ternary complex with dGTP-($\beta-\gamma$ CH_2), as determined by single-crystal X-ray diffraction, indicates that the triphosphate region of the native, bound dNTP (*37*, *38*) and the corresponding region of the analogue superimpose with virtually no deviation (Figure 3A). The β,γ-bridging position protrudes into a solvent-accessible region, and no steric interactions with surrounding protein moieties are observed. Importantly, no energetically significant perturbation of the positions of catalytic metal cations or active site aspartate residues is observed. In Figure 3B, the structures of dGTP($\beta-\gamma$ CF_2) and dGTP($\beta-\gamma$ CH_2) are compared, likewise revealing nearly identical superimpositions and lack of active site perturbation.

Structures like those depicted in Figure 3 represent, of course, only one of the possible conformational states in the reaction. However, the K_ds for the correct-pairing analogue−enzyme ternary complexes (Table 3, discussed below) are all on par with the K_d for the native complex. Since similar K_d values reflect a similarity in all of the conformational states of the binding equilibria prior to chemistry, these data support an LFER treatment of the reaction kinetics.

Kinetic Assays Reveal a "Broken" LFER. The parameters k_{pol} and K_d were obtained in transient-kinetic experiments as described in Materials and Methods. Since experimental uncertainty in the values of k_{pol} can have a large effect on the slope of a Brønsted plot, a high degree of precision in the gap-filling assay is desirable. Figure 4 displays representative data from a single assay and demonstrates that the quantification of k_{obs}([S]) and $[P]_t$ are excellent fits to the kinetic equations. The best-fit values for k_{pol} and K_d, and the fidelity parameters derived from them, are tabulated in Table 3. The standard error of the mean of three replicates in k_{pol} was typically 7%.

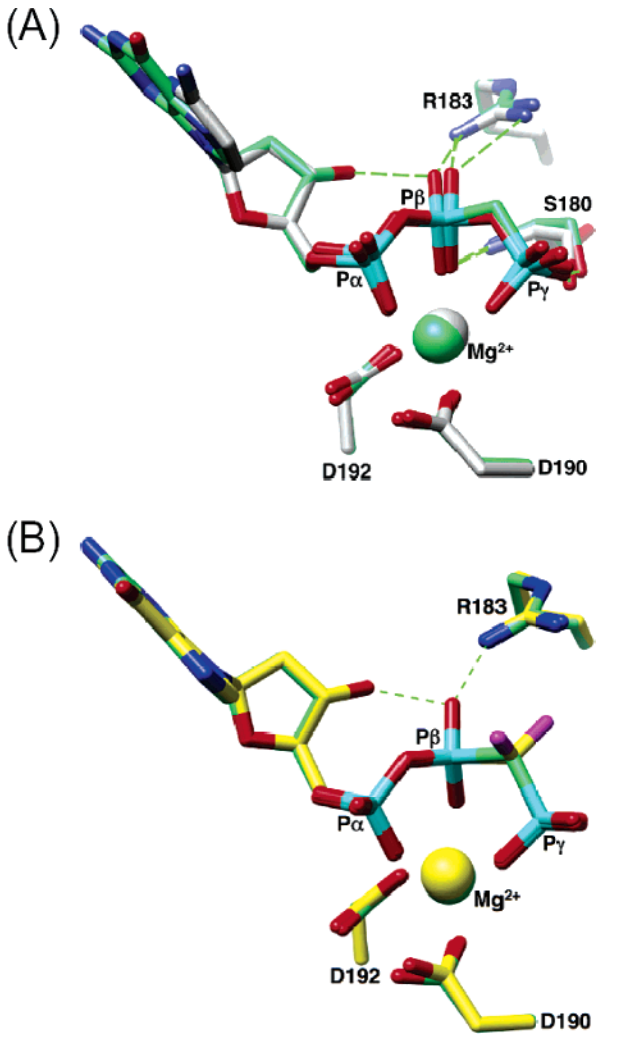

FIGURE 3: Structure of native and analogue conformations bound to pol β. (A) Ternary complex structures of pol β with dCTP (*37*) (gray) or a dGTP analogue (green, Table 1) where $O_{\beta\gamma}$ has been replaced with a methylene (CH_2) group are superimposed. A nonbridging oxygen on the β-phosphate forms hydrogen bonds with O3′ of the incoming nucleotide as well as Ser180 (S180) and Arg183 (R183). Active site aspartates (D190 and D192) and the nucleotide-coordinating Mg^{2+} are also shown. (B) Ternary complex structures of pol β with dGTP analogues where the β,γ-bridging oxygen is replaced by a methylene (CH_2, green) or difluoromethylene (CF_2, yellow). The superimposed structures indicate that the β,γ substituents do not perturb the active site structure. Graphics were prepared using Chimera (*38*).

The Brønsted equation as it pertains to leaving-group (lg) ability

$$\log(k_{pol}) = \beta_{lg}(pK_{a,lg}) + \text{constant} \qquad (1)$$

was first developed as an empirical observation of the dependence of the catalytic rate constant on the intrinsic reactivity of the substrate, where leaving-group pK_a is taken as a reference for the intrinsic reactivity. A linear relationship between reactivity and pK_a has since been found to hold for a diverse set of reactions including alkyl (*39*), halo (*39*), and phosphoryl (*12*, *13*) transfers.

As presented above, structural and K_d evidence suggests that the (halo)methylene groups that replace $O_{\beta\gamma}$ have little effect on the conformation and energetics of the substrate binding portion of the mechanism. Another important

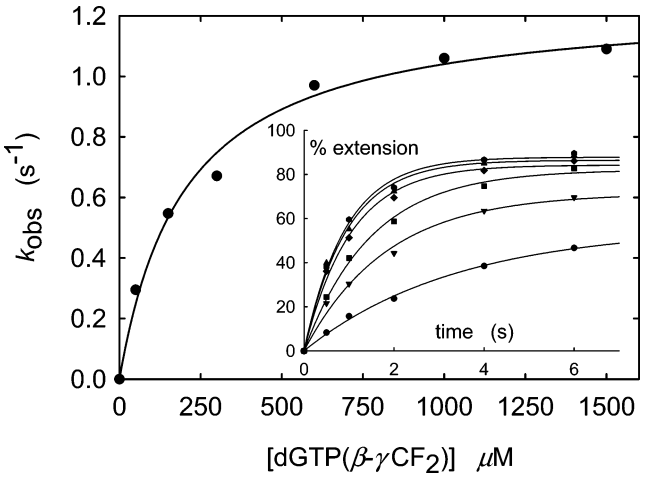

FIGURE 4: Single-turnover assay of dGTP($\beta-\gamma$ CF_2) insertion opposite template T, showing saturation of the observed single-exponential rate constant, k_{obs}, as a function of substrate concentration. Plots of k_{obs} versus substrate concentration were least-squares fit to the hyperbolic equation (Materials and Methods) to obtain the best-fit catalytic rate constant k_{pol} and the substrate dissociation constant K_d. Inset: The percentage of ^{32}P 5′-end-labeled primer extended during the course of the nucleotidyl transfer reactions. The curves are the best least-squares fits of the data to a single exponential, yielding k_{obs} at each substrate concentration. Experiments were done in triplicate for all substrates opposite template C or T, and the results are tabulated in Table 3. The plots here are representative of the typical signal-to-noise ratios and fluctuations observed in the data acquisition.

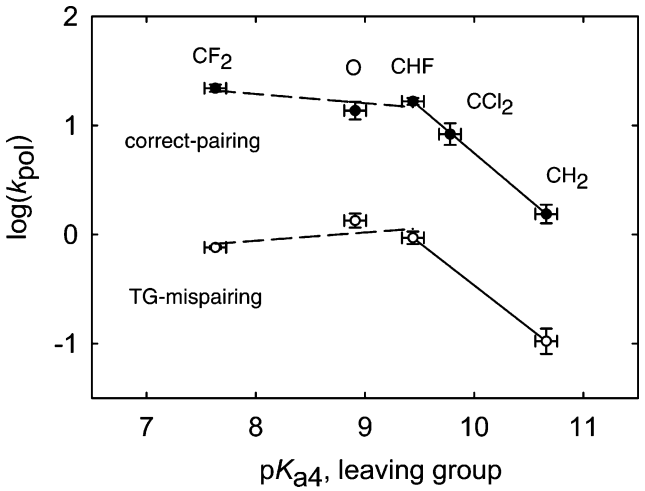

FIGURE 5: Brønsted correlations of log(k_{pol}) to the pK_{a4} values reported in Table 2. The error bars represent ± 2 SD log(k_{pol}) and ± 0.1 pK_{a4}. Both correct-pairing (top) and T·G-mispairing (bottom) assays show a region of catalytic sensitivity to leaving-group pK_a in the domain 9−11 (between the CHF and CH_2 analogues). β_{lg}(correct) = −0.84; β_{lg}(T·G-mispair) = −0.78. These values are similar to β_{lg}s reported for other enzymatic P−O cleavage reactions (*12*, *13*). In the pK_a domain 7.5−9 (between CF_2 and CHF analogues) a region of catalytic insensitivity exists for both curves. The data point for the sterically large CCl_2 analogue (studied opposite template C) is collinear with CH_2 and CHF. These data and structural (Figure 3) and equilibrium (Table 3) data opposite the same template suggest that the flat position of the CF_2 point is due to sufficient stabilization of leaving-group elimination such that an earlier activation barrier becomes rate-limiting.

observation from Figure 3 and other structural data is that the carbon−hydrogen or carbon−halogen bonds are directed into a relatively solvent-exposed region and away from the divalent metal cations, so complicating effects on pK_a that could arise from preferential M^{2+} coordination with the halogens, versus the methylene hydrogens, should be absent. If all β,γ-bridging groups (oxygen lone pairs, carbon−hydrogen bonds, carbon−halogen bonds) experience the same environment in the active site, leaving-group pK_a values in the protein, while possibly differing in absolute value, can reasonably be expected to follow the same trend as in solution (Table 2). In such a case, the shape of a Brønsted correlation would not change. Effective pK_a values of leaving groups bound in the active site are ideal but would be difficult to obtain; in their absence the use of Table 2 values is justified.

Brønsted plots for correct-pairing and T·G-mispairing assays are shown in Figure 5. In both cases, a region of catalytic sensitivity to leaving-group pK_a is observed in the pK_a domain 9−11 (between the CHF and CH_2 analogues). The two slopes in this region are similar (β_{lg}, correct = −0.84; β_{lg}, T·G mispair = −0.78). Catalytic sensitivities of this magnitude, over a roughly 2-unit pK_a range, have been reported for phospholipase C (*13*); moreover, β_{lg}s ≈ −0.8 have been reported for other enzymatic P−O cleavage reactions (*12*, *13*). An interesting result from this work, however, is the virtually flat portions of both curves between pK_a 7.5−9 (from CF_2 to CHF analogues). The transition to catalytic insensitivity occurs at roughly the same point for both correct and T·G-mispairing assays, close to the pK_a of the native oxo-bridging compound.

A break in the linearity of a Brønsted plot is often taken to mean a change in the mechanism of a solution phase reaction (*40*). In a multistep mechanism probed by substituent effect stabilization of a single barrier, where the log(k) dependence on pK_a goes from zero slope to significant negative slope (with increasing pK_a), it can mean that at the pK_a of the discontinuity there is a transition point between two different rate-limiting steps. As will be illustrated below, a zero slope region can arise when there exist two transition states of similar heights, among other possibilities. At pK_as left of the discontinuity (weaker base, stronger electron-withdrawing ability) the step that is more weakly influenced by electron withdrawal dominates. The biphasic LFER plots we obtain suggest such an interpretation.

Comparison of the CF_2 data point with that of CCl_2 (assayed opposite template C) lends further support to the structural and K_d data suggesting that the effect of $O_{\beta\gamma}$ replacement is primarily a stabilization of leaving-group elimination and not steric/electrostatic perturbations. Sterically, the CCl_2 group has a significantly larger profile than CF_2. That the CCl_2 point should fall collinear with CH_2 and CHF, with a β_{lg} in the range reported for other enzymatic P−O cleavages, while the sterically smaller CF_2 not only deviates from that slope but shows virtually zero slope behavior strongly suggests that the breaks in Figure 5 can be explained by a leaving-group-induced change in the rate-limiting step. We use the EVB free energy perturbation simulations to calculate structures and energies of states along the reaction coordinate, information that cannot be obtained by experiment. We explore how these calculations can lend additional insight into the experimental results.

Theoretical and Computational Analysis Predicts a Nonlinear Brønsted Relationship. The insertion of dGTP analogues containing O, CF_2, and CH_2 β,γ-bridging groups opposite C in the template was simulated using the EVB/

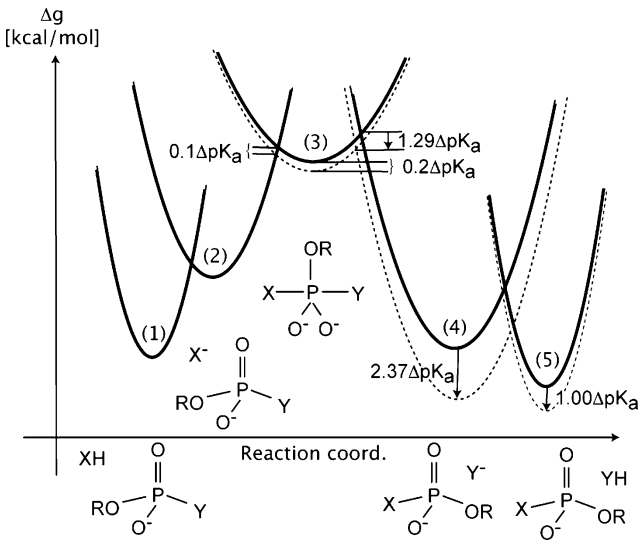

FIGURE 6: Free energy diagram depicting the intermediates (diabatic states approximated by Marcus' parabolas) along a stepwise nucleotidyl transfer reaction in aqueous solution, where X denotes the nucleophile. The free energy changes at 298 K caused by a substitution of the leaving group (Y) that lowers its pK_a are indicated by arrows and dashed parabolas. The selection of numerical values for changes in the free energies of states 3, 4, and 5 (i.e., Brønsted coefficients β_{eq}) and for the intersections of these states (β_{lg}) is described in the Supporting Information.

FEP approach (*25*). Calculations were performed in aqueous solution (Supporting Information, Figure 3S) and in pol β. However, due to the nature of the EVB method, only the results for the reactions in the protein can be considered "parameter-free". This is because the EVB free energies in water are forced to reproduce the observed and/or high-level quantum mechanical energetics by adjusting empirical constants in the EVB Hamiltonian (Supporting Information, Table 1S). Thus, the energetics of the model reaction in water and assumptions made about these energetics (*41*) are important factors underlying the results of EVB calculations of chemical reactions in proteins.

The model free energy surface assumed for the multistep reaction of substituted dNTP compounds in water is presented in Figure 6. This surface is based on intersecting parabolas representing the free energies of the steps outlined in Figure 6; intersections with the highest energy correspond to the rate-limiting transition state. The relative position of the parabolas plays a crucial role since it determines the height of their intersections. More specifically, according to the modified Marcus relationship (Supporting Information, eq 2S), the shift of the vertical position (i.e., free energy) of the intersection of each pair of parabolas is linearly proportional to the change in the relative position of their minima. When this proportionality is determined (as described in detail in Supporting Information and in ref *42*) for each microscopic reaction step of a stepwise associative nucleotidyl transfer reaction, we obtain the model free energy surface of Figure 6. This conceptual framework predicts the observation of a "break" in the LFER due to a change in the rate-limiting step of the nucleotide insertion reaction. This conclusion holds even if the curvatures of the various parabolas are different, but the predicted β_{lg} is based on the assumption of equal curvatures.

The actual parabolas and their mixing can be determined by the EVB approach as discussed elsewhere (*11*). Thus, in addition to introducing the free energy model of Figure 6, we quantified the general trend of the LFER in solution by simple parametric EVB calculations. The results of this parametric approach are presented in Supporting Information, Figure 2S. We believe that Figure 2S represents a best current estimate of the LFER in solution and consider it as a useful theoretical guide. Interestingly, the results presented in Figure 2S can be converted to β_{lg} of -0.87. This value falls between the slope observed for model compounds in aqueous solution ($\beta_{lg} = -0.94$) (*43*) and $\beta_{lg} = -0.84$ observed in the protein.

To further extend the theoretical LFER model, we carried out parameter-free EVB/FEP simulations of the $2 \rightarrow 3 \rightarrow 4$ (Figure 6) microscopic reaction steps in pol β. These calculations include contributions from all interactions of the substrate with the protein environment during the reaction. Since there is uncertainty about the actual profile and degree of concertedness (Figure 1) of the model reaction in water (*35*), which represents the foundation all protein EVB simulations, we carried out two independent EVB studies.

Initially, we used a stepwise associative reference free energy surface in water that coincided with the surface used in previous EVB simulations of the reaction mechanism and fidelity of T7 DNA polymerase (*8*, *41*). Applying this model (Figures 1B and 6) to pol β, the nucleophilic attack step was found to be the slowest microscopic chemical step in the protein for all three substrates (TS1 > TS2; Supporting Information, Figure 5S), and the calculated relative rate constants (Supporting Information, Table 2S) were inconsistent with the observed LFER (Figure 5). Nevertheless, these calculations may reveal an important difference between the catalytic mechanism of pol β and T7 pol in that the nucleophilic step is less stabilized in pol β than in T7 pol. This difference is likely caused by stabilizing electrostatic interactions contributed by the Lys522 residue and by a larger flexibility in the positioning of the "catalytic" Mg^{2+} in T7 pol (*8*). The structural equivalent of the positively charged Lys522, which interacts with one of the nonbridging oxygens of the α-phosphate, is missing in pol β.

To reconcile this inconsistency with the observed LFER, we assumed a concerted reaction with a "late" transition state in water (Figure 7). On the basis of the EVB parametrization for this reference reaction, β_{lg} of -0.73 was calculated for dGTP and dGTP($\beta-\gamma$ CH_2). This β_{lg}, although obtained by parameter-free simulations in the protein, is close to β_{lg} of -0.84 observed in our transient-kinetic experiments. A break in linearity, which is consistent with data in Figure 5, was calculated for the CF_2 analogue. The reaction of this analogue is associated with slightly higher activation free energy than for the native substrate (Figure 7, Table 2S). This activation free energy increase is dominated by an intramolecular steric or electrostatic repulsion (Supporting Information, Movie 1S and Figure 4S), which destabilizes both TS1 and TS2 transition states (Figure 7). However, this result appears to reflect a difficulty in attaining a more precise energy balance in the system, because the experiments for the analogue containing a larger CCl_2 group indicate the absence of a significant steric effect on the observed rate constants (Figure 5).

Despite this drawback, the analysis of trajectories and free energies calculated for both models (concerted Figure 1A or stepwise Figure 1B) shows absence of any protein−substrate steric effects affecting CH_2 or CF_2 analogues.

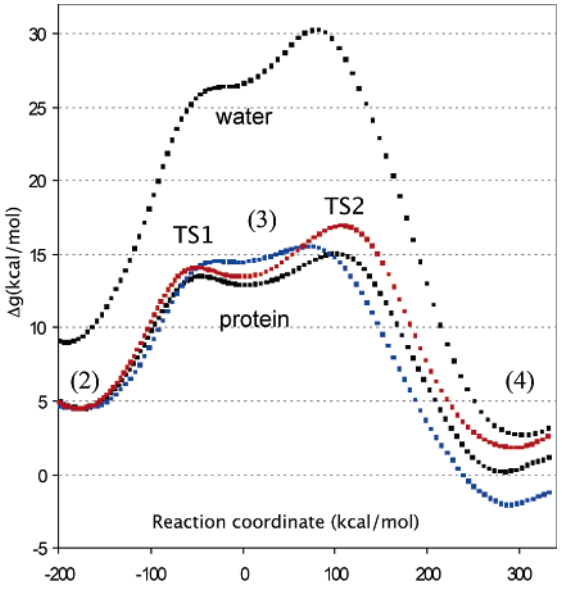

FIGURE 7: EVB/FEP free energy surfaces for the nucleophilic attack and $P_\alpha - O_{\alpha\beta}$ bond-breaking steps of the nucleotidyl transfer reaction in pol β. The EVB parameters were obtained by assuming the concerted free energy profile for the reference reaction in water (upper black curve). The black, red, and blue curves denote the insertion of dGTP, dGTP($\beta-\gamma$ CH_2), and dGTP($\beta-\gamma$ CF_2), respectively, opposite C in the template. The zero of the free energy scale in both water and the protein was assigned to state 1 (Figure 6), which is not shown in the graph.

Moreover, the correct LFER was obtained for the native substrate and the CH_2 analogue when the concerted reference reaction in aqueous solution was assumed. Even in this case, however, the resulting free energy profile in the protein was stepwise (Figure 7) and similar to the model depicted in Figure 6. The change in the character of the free energy profile from a single TS (concerted profile) to a stepwise profile featuring dianionic pentavalent intermediate flanked by TS1 and TS2 transition states is due to stronger protein binding to TS2 and the pentavalent intermediate than TS1.

$O_{\beta\gamma}$ Replacement Has Only Subtle Effects on Fidelity, with the Exception of the CH_2 Analogue. We have measured incorporation of dGTP (or analogue) opposite two template bases, C and T, and consider the effect of $O_{\beta\gamma}$ replacement on the misinsertion frequency, f_{ins}, which is inversely proportional to fidelity, and for a T·G mispair is given by (*44*)

$$f_{ins,TG} = \frac{(k_{cat}/K_M)_{TG}}{(k_{cat}/K_M)_{CG}} \approx \frac{(k_{pol}/K_d)_{TG}}{(k_{pol}/K_d)_{CG}} = \left(\frac{k_{pol,TG}}{k_{pol,CG}}\right)\left(\frac{K_{d,TG}}{K_{d,CG}}\right)^{-1} \quad (2)$$

where k_{cat}/K_M is the steady-state efficiency, or specificity constant (*45*), and pre-steady-state or single-turnover measurements of k_{pol}/K_d provide a very close approximation (*3*, *46*). In the rightmost term above, $f_{ins,TG}$ is rearranged to be written as contributions from separate catalytic ($k_{pol,TG}/k_{pol,CG}$) and substrate-binding ($K_{d,TG}/K_{d,CG}$) terms.

In calculating $f_{ins,TG}$, we are observing a "template-variable" selectivity, which is not the situation in vivo, where the dNTP is the variable and the template is constant. Since the environment of the template base and that of the dNTP are different in the active site, selectivity measured by these two methods may not be the same. In either case, however, the enzyme preferentially catalyzes the correct-pairing reaction, so template-variable selectivity is a valid probe of polymerase mechanisms. Our reason for measuring fidelity in this manner is to make a best comparison of experiment with theory. The computational studies use a template variable model to minimize inaccuracies in calculated parameters (*47*). Contributions to $f_{ins,TG}$ are graphed in Figure 8, relative to the same terms for the native compound.

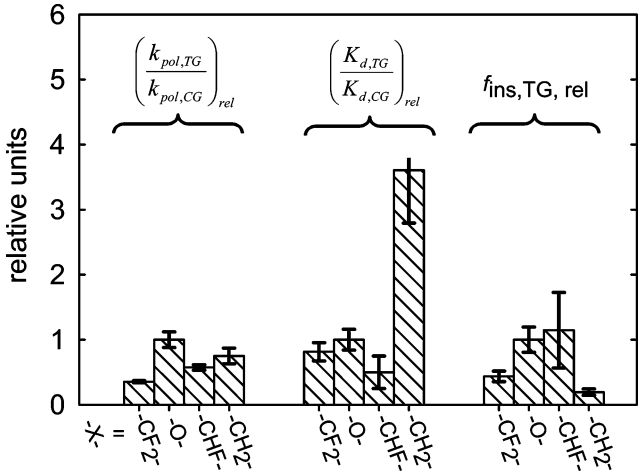

FIGURE 8: Substituent effect on fidelity. The ratios $(k_{pol,TG}/k_{pol,CG})_{-X-}$ and $(K_{d,TG}/K_{d,CG})_{-X-}$, plotted relative to the same terms for the native substrate, account for contributions to f_{ins} (eq 2) from catalysis and substrate binding, respectively. Error in the relative quantities is propagated according to standard rules for propagation of error. Replacing $O_{\beta\gamma}$ with CH_2 leads to an ~4-fold larger binding term, a significant contribution to the relative fidelity of that analogue. Because the Brønsted plots show similar trends for both C·G correct pair and T·G-mispair incorporation, contributions from the catalytic term are relatively small (discussed in the text).

Because the shape of the Brønsted plots for both correct pair and T·G mispair incorporation are quantitatively similar (Figure 5), contributions to $f_{ins,TG}$ from the catalytic term should be small. This is in fact observed in Figure 8. Note for example that, from Table 3, the CH_2 analogue has reduced k_{pol} values for both correct and T·G mispair incorporation. This k_{pol} decrease (relative to native) is comparable opposite both templates, such that the contribution to fidelity is small. Although the catalytic terms for the CHF and CF_2 analogues are somewhat lower than for native, these can be attributed to small deviations from the near-zero-slope lines in Figure 5, resulting from experimental variability in the measurement of k_{pol}. In terms of binding, the only possibly significant effect appears to be from the CH_2 analogue, which binds ~2-fold better opposite C and ~2-fold worse opposite T compared with dGTP (Table 3). Owing principally to these rather small differential binding effects, pol β discriminates against making T·G mispairs somewhat better with the CH_2 analogue than with the native substrate.

DISCUSSION

Herein we have presented structural and equilibrium data to demonstrate that replacing the β,γ-bridging triphosphate oxygen with (halo)methylene groups is a noninvasive modification in terms of substrate binding in the pol β active site. This evidence argues strongly in favor of an LFER interpretation of the single-turnover transient kinetics correlating $\log(k_{pol})$ with leaving-group pK_a. The series of

modifications exhibit diverse steric/electrostatic profiles (cf. CH_2, CF_2, CCl_2) and cover a significant (~3 unit) pK_a range. The location of the breaks relative to pK_as of CF_2, O, and the sterically bulky CCl_2-bridging compounds suggests that the biphasic nature of the Brønsted correlations is due to a modification-induced change in the mechanism by stabilization of leaving-group elimination. EVB/FEP calculations using atomic coordinates from ternary complexes of the same system predict trajectories in agreement with this interpretation, via stabilization of a late activation barrier in a stepwise model (Figure 1). Lastly, due largely to the similar shape of the Brønsted correlations for both correct and T·G-mispairing assays, the effect of leaving-group modification on fidelity is subtle. Significantly greater discrimination with the CH_2 analogue can be explained in terms of a differential binding effect.

The observation of significant changes in k_{pol} in the pK_a range 9−11 provides direct evidence that the activation barrier for bond breaking at the scissile $P_\alpha-O_{\alpha\beta}$ has larger or equal height relative to other barriers along the reaction coordinate for pol β-catalyzed nucleotidyl transfer of dGTP opposite template C or T. The approximate position of the breaks in Figure 5, close to the pK_a of the native compound, suggests, however, that an earlier barrier lies close in energy. The MD simulations performed here for pol β, and other work with T7 polymerase (*8*), suggest this to be the nucleophilic bond-forming step. This result supports the view that chemistry, and not conformational change, is rate-limiting for both correct and misincorporation processes catalyzed by pol β (*48*, *49*).

Our conclusion that the altered kinetic profile can be attributed to changes in the chemical step is further supported by the observation that there are negligible close contacts between the protein residues and the β,γ-bridging group of the substrate bound in the active site (Figure 3). In the absence of such contacts, and in view of the similarity of the electrostatic potentials of the native and modified substrates, substitution at the β,γ-bridging position is unlikely to affect the rate of conformational changes. If the conformational changes before chemistry were in fact rate-limiting, the observed reaction rate constant, k_{pol}, should be insensitive to replacement of dGTP by the analogues. Instead, for the insertion of both the correct and incorrect substrate, a significant difference in k_{pol} was observed.

The similarity of the observed Brønsted correlations (Figure 5) for the correct (C·G) and incorrect (T·G) insertion raises the possibility that the positions of the catalytic and structural Mg^{2+} ions, and the contacts of the protein residues with the α-, β-, and γ-phosphates of the bound substrate, are conserved in misincorporation, in the sense that $P_\alpha-O_{\alpha\beta}$ bond cleavage is rate-limiting for insertion of the CH_2 analogue opposite either C or T in the template. This observation appears inconsistent with attribution of pol β fidelity to a less efficient positioning of the so-called catalytic Mg^{2+} ion for the insertion of incorrect dNTP, because such a structural change would likely result in a significantly higher TS1 than TS2. In this case, the LFER for the mispair would be characterized by β_{lg} close to zero for all analogues, which was not observed. Since the misinsertion of dGTP opposite a template T is the least perturbing mispair formed as deduced from the pol β specificity constants (*50*), only minor effects on catalytic metal binding would be expected. However, there is a second "structural" Mg^{2+} ion, whose position can and probably will change and contribute to fidelity. Most importantly, the similarity in the observed β_{lg} for the correct and incorrect insertion is consistent with incorrect insertion occurring from a partially open conformation, if such a conformation difference increases TS2 more than TS1 (Figure 7). This is plausible because the interactions of the Arg183 and Ser180 residues with the β- and γ-phosphates, respectively, are weakened in the partially open conformation (*5*). These findings are important because further progress in the quantitative calculations of DNA polymerase fidelity critically depends on identification of the partially open conformation for incorrect insertion (*41*).

The all-atom EVB/FEP MD calculations in the protein suggest that the catalytic effect of the protein is similar for each leaving-group analogue, despite the possibility that steric interactions of the protein with the CF_2- or CH_2-bridging groups might lead to significant changes in the orientation of the reacting substrate during the reaction. We would propose, therefore, that the change in pK_as in the protein is likely similar to the corresponding change in solution and that the computational analysis, embodied in Figures 6 and 7, offers a credible, qualitative basis to grasp how the rate-determining step in pol β can change as a function of the leaving-group pK_a.

The chemical transformation necessary for dNTP insertion by a polymerase likely involves three microscopic chemical steps: proton transfer, nucleophilic attack, and formation of the leaving group (i.e., $P_\alpha-O_{\alpha\beta}$ bond breaking). While proton transfer is an unlikely candidate for the slowest step (*41*), the other two steps are expected to be of similar height (*41*). If the activation barrier for bond breaking were significantly lowered, as expected with the CF_2 analogue, deprotonation and/or nucleophilic attack may become sensitive to a kinetic isotope effect. The experiments reported here are a necessary prelude to such studies, and experiments of the type described here may be expanded to include other functional group modifications at $O_{\beta\gamma}$ and other polymerases where nucleotidyl transfer may be more rapid (non-rate-limiting) than proposed conformational change steps.

ACKNOWLEDGMENT

C.E.M. thanks Dr. Ron New of the University of California, Riverside, Mass Spectrometry Laboratory for assistance in obtaining HRMS spectra of dNTP analogues and Prof. P. Qin for use of his UV−visible spectrophotometer to determine dNTP concentrations. We also thank Dr. George Kenyon, University of Michigan, for generous sharing of ideas and techniques and for providing valuable constructive criticism and encouragement to all the members of our Program Project.

SUPPORTING INFORMATION AVAILABLE

A detailed EVB/FEP methodology, including force field and Hamiltonian parameters; a derivation of the LFER equations and modified Marcus relation; EVB/FEP results in aqueous solution and assuming different stepwise or concerted free energy surfaces in the protein; calculated free energy surfaces in pol β for the EVB parametrization using stepwise reference surface in water; a graph of the variation of the $F-O_{\alpha\beta}$ distance; a movie of dGTP($\beta-\gamma$ CF_2)

dynamics in the pol β active site during the initial part of nucleophilic attack. This material is available free of charge via the Internet at http://pubs.acs.org.

REFERENCES

1. Goodman, M. F. (2002) Error-prone repair DNA polymerases in prokaryotes and eukaryotes, *Annu. Rev. Biochem. 71*, 17−50.
2. Arndt, J. W., Gong, W., Zhong, X., Showalter, A. K., Liu, J., Dunlap, C. A., Lin, Z., Paxson, C., Tsai, M. D., and Chan, M. K. (2001) Insight into the catalytic mechanism of DNA polymerase β: structures of intermediate complexes, *Biochemistry 40*, 5368−5375.
3. Beard, W. A., and Wilson, S. H. (2006) Structure and mechanism of DNA polymerase β, *Chem. Rev. 106*, 361−382.
4. Wilson, S. H. (1998) Mammalian base excision repair and DNA polymerase β, *Mutat. Res. 407*, 203−215.
5. Sawaya, M. R., Pelletier, H., Kumar, A., Wilson, S. H., and Kraut, J. (1994) Crystal structure of rat DNA polymerase β: Evidence for a common polymerase mechanism, *Science 264*, 1930−1935.
6. Pelletier, H., Sawaya, M. R., Kumar, A., Wilson, S. H., and Kraut, J. (1994) Structures of ternary complexes of rat DNA polymerase β, a DNA template-primer, and ddCTP, *Science 264*, 1891−1903.
7. Sawaya, M. R., Prasad, P., Wilson, S. H., Kraut, J., and Pelletier, H. (1997) Crystal structures of human DNA polymerase β complexed with gapped and nicked DNA: Evidence for an induced fit mechanism, *Biochemistry 36*, 11205−11215.
8. Florián, J., Goodman, M. F., and Warshel, A. (2003) Computer simulation of the chemical catalysis of DNA polymerases: Discriminating between alternative nucleotide insertion mechanisms for T7 DNA polymerase, *J. Am. Chem. Soc. 125*, 8163−8177.
9. Benkovic, S. J., and Schray, K. J. (1973) The chemistry of phosphoryl transfer, in *The Enzymes* (Boyer, P. D., Ed.) p 201, Academic Press, New York.
10. Braun-Sand, S., Olsson, M. H. M., and Warshel, A. (2005) Computer modeling of enzyme catalysis and its relationship to concepts in physical organic chemistry, *Adv. Phys. Org. Chem. 40*, 201−245.
11. Warshel, A., Hwang, J. K., and Aqvist, J. (1992) Computer simulations of enzymatic reactions: Examination of linear free energy relationships and quantum mechanical corrections in the initial proton-transfer step of carbonic anhydrase, *Faraday Discuss. 93*, 225−238.
12. Hollfelder, F., and Herschlag, D. (1995) The nature of the transition state for enzyme-catalyzed phosphoryl transfer. Hydrolysis of O-aryl phosphorothioates by alkaline phosphatase, *Biochemistry 34*, 12255−12264.
13. Mihai, C., Kravchuk, A. V., Tsai, M. D., and Bruzik, K. S. (2003) Application of Bronsted-type LFER in the study of the phospholipase C mechanism, *J. Am. Chem. Soc. 125*, 3236−3242.
14. Silverman, D. N., Tu, C., Chen, X., Tanhauser, S. M., Kresge, A. J., and Laipis, P. J. (1993) Rate-equilibria relationships in intramolecular proton transfer in human carbonic anhydrase III, *Biochemistry 32*, 10757−10762.
15. Moffatt, J. G., and Khorana, H. G. (1961) Nucleoside polyphosphates. X. The synthesis and some reactions of nucleoside 5′-phosphoromorphoilidates and related compounds. Improved methods for the preparation of nucleoside 5′-polyphosphates, *J. Am. Chem. Soc. 83*, 649−658.
16. Arabshahi, L., Khan, M. M., Butler, M., Noonan, T., Brown, N. C., and Wright, G. E. (1990) (Difluoromethylene)phosphates of guanine nucleosides as probes of DNA polymerase and G proteins, *Biochemistry 29*, 6820−6826.
17. Beard, W. A., and Wilson, S. H. (1995) Purification and domain-mapping of mammalian DNA polymerase β, *Methods Enzymol. 262*, 98−107.
18. Otwinowski, Z., and Minor, W. (1997) Processsing of x-ray diffraction data collected in oscillation mode, *Methods Enzymol. 276*, 307−326.
19. Kleywegt, G. J., and Jones, T. A. (1997) Model building and refinement practice, *Methods Enzymol. 277*, 208−231.
20. Jones, T. A., Zou, J. Y., Cowan, S. W., and Kjeldgaard (1991) Improved methods for binding protein models in electron density maps and the location of errors in these models, *Acta Crystallogr. A 47*, 110−119.
21. Burton, D. J., Pietrzyk, D. J., Ishihara, T., Fonong, T., and Flynn, R. M. (1982) Preparation, stability and acidity of difluoromethylenebisphosphonic acid, *J. Fluorine Chem. 20*, 617−626.
22. Daniele, P. G., Rigano, C., and Sammartano, S. (1985) Ionic strength dependence of formation constants. Alkali metal complexes of ethylenediaminetetraacetate nitrilotriacetate, diphosphate, and tripolyphosphate in aqueous solution, *Anal. Chem. 57*, 2956−2960.
23. Leswara, N. D. (1982) *-fluoromethanediphosphonic acids and derived ATP analogs, Ph.D. Thesis, Department of Chemistry, University of Southern California, Los Angeles.
24. Claessens, R. A. M. J., and Van der Linden, J. G. M. (1984) Stability constants of tin(II) and calcium diphosponate complexes, *J. Inorg. Biochem. 21*, 73−82.
25. Warshel, A., and Florián, J. (2004) The empirical valence bond (EVB) method, in *The Encyclopedia of Computational Chemistry* (Schleyer, P. v., Jorgensen, W. L., Schaefer, H. F., III, Schreiner, P. R., Thiel, W., and Glen, R., Eds.) John Wiley & Sons, Chichester, U.K.
26. Cornell, W. D., Cieplak, P., Bayly, C. I., Gould, I. R., Merz, K. M., Jr., Ferguson, D. M., Spellmeyer, D. C., Fox, T., Caldwell, J. W., and Kollman, P. A. (1995) A second generation force field for the simulation of proteins, nucleic acids, and organic molecules, *J. Am. Chem. Soc. 117*, 5179−5197.
27. Marelius, J., Kolmodin, K., Feierberg, I., and Åqvist, J. (1999) Q: A molecular dynamics program for free energy calculations and empirical valence bond simulations in biomolecular systems, *J. Mol. Graphics Modell. 16*, 213−225.
28. Reynolds, W. F. (1983) Polar substituent effects, *Prog. Phys. Org. Chem. 14*, 165−203.
29. Taft, R. W., and Topsom, R. D. (1987) The nature and analysis of substituent electronic effects, *Prog. Phys. Org. Chem. 16*, 1−84.
30. Albery, W. J. (1980) The application of the Marcus relation to reactions in solution, *Annu. Rev. Phys. Chem. 31*, 227−263.
31. Hassid, A. I., Kreevoy, M. M., and Liang, T. M. (1975) The reaction complex in proton transfer, *Faraday Symp. Chem. Soc. 10*, 69−77.
32. Schweins, T., Geyer, M., Kalbitzer, H. R., Wittinghofer, A., and Warshel, A. (1996) Linear free energy relationships in the intrinsic and GTPase activating protein-stimulated guanosine 5′-triphosphate hydrolysis of p21ras, *Biochemistry 35*, 14225−14231.
33. Berkowitz, D. B., and Bose, M. (2001) (α-Monofluoroalkyl)-phosphonates: a class of isoacidic and "tunable" mimics of biological phosphates, *J. Fluorine Chem. 112*, 13−33.
34. McKenna, C. E., and Shen, P. (1981) Fluorination of methanediphosphonate esters by perchloryl fluoride. Synthesis of fluoromethanediphosphonic acid and difluoromethanediphosphonic acid, *J. Org. Chem. 46*, 4573−4576.
35. Blackburn, G. M., Kent, D. E., and Kolkmann, F. (1984) The synthesis and metal binding characteristics of novel, isopolar phosphonate analogs of nucleotides, *J. Chem. Soc., Perkin Trans. 1*, 1119−1125.
36. Cotton, F. A., Wilkinson, G., and Gaus, P. L. (1995) *Basic Inorganic Chemistry*, John Wiley and Sons, New York.
37. Batra, V. K., Beard, W. A., Shock, D. D., Krahn, J. M., Pedersen, L. C., and Wilson, S. H. (2006) Magnesium induced assembly of a complete DNA polymerase catalytic complex, *Structure 14*, 757−766.
38. Pettersen, E. F., Goddard, T. D., Huang, C. C., Couch, G. S., Greenblatt, D. M., Meng, E. C., and Ferrin, T. E. (2004) UCSF Chimera−A visualization system for exploratory research and analysis, *J. Comput. Chem. 25*, 1605−1612.
39. Bordwell, F. G., Cripe, T. A., and Hughes, D. L. (1987) Nucleophilicity, basicity, and the Bronsted equation, in *Nucleophilicity (Advances in Chemistry Series*) (Harris, J. M., and McManus, S. P., Eds.) pp 137−153, Amercian Chemical Society, Washington, DC.
40. Jencks, W. P. (1987) Effects of solvation on nucleophilic reactivity in hydroxylic solvents: Decreasing reactivity with increasing basicity, in *Nucleophilicity (Advances in Chemistry Series*) (Harris, J. M., and McManus, S. P., Eds.) pp 155−167, Amercian Chemical Society, Washington, DC.
41. Florián, J., Goodman, M. F., and Warshel, A. (2005) Computer simulations of protein functions: Searching for the molecular origin of the replication fidelity of DNA polymerases, *Proc. Natl. Acad. Sci. U.S.A. 102*, 6819−6824.
42. Åqvist, J., Kolmodin, K., Florián, J., and Warshel, A. (1999) Mechanistic alternatives in phosphate monoester hydrolysis: What

conclusions can be drawn from available experimental data?, *Chem. Biol. 6*, R71−R80.
43. Zalatan, J. G., and Herschlag, D. (2006) Alkaline phosphate mono- and diesterase reactions: Comparative transition state analysis, *J. Am. Chem. Soc. 128*, 1293−1303.
44. Goodman, M. F., Creighton, S., Bloom, L. B., and Petruska, J. (1993) Biochemical basis of DNA replication fidelity, *Crit. Rev. Biochem. Mol. Biol. 28*, 83−126.
45. Fersht, A. R., Knill-Jones, J. W., and Tsui, W. C. (1982) Kinetic basis of spontaneous mutation: Misinsertion frequencies, proof-reading specificities and cost of proofreading by DNA polymerases of *Escherichia coli*, *J. Mol. Biol. 156*, 37−51.
46. Johnson, K. A. (1993) Conformational coupling in DNA polymerase fidelity, *Annu. Rev. Biochem. 62*, 685−713.
47. Florián, J., Goodman, M. F., and Warshel, A. (2002) Theoretical investigation of the binding free energies and key substrate-recognition components of the replication fidelity of human DNA polymerase β, *J. Phys. Chem. B 106*, 5739−5753.
48. Bakhtina, M., Lee, S., Wang, Y., Dunlap, C., Lamarche, B., and Tsai, M. D. (2005) Use of viscogens, dNTPaS, and rhodium(III) as probes in stopped-flow experiments to obtain new evidence for the mechanism of catalysis by DNA polymerase β, *Biochemistry 44*, 5177−5187.
49. Dunlap, C. A., and Tsai, M. D. (2002) Use of 2-aminopurine and tryptophan fluorescence as probes in kinetic analyses of DNA polymerase β, *Biochemistry 41*, 11226−11235.
50. Beard, W. A., Shock, D. D., and Wilson, S. H. (2004) Influence of DNA structure on DNA polymerase β active site function: Extension of mutagenic DNA intermediates, *J. Biol. Chem. 279*, 31921−31929.
51. Lovell, S. C., Davis, I. W., Arendall, W. B., III, de Bakker, P. I. W., Word, J. M., Prisant, M. G., Richardson, J. S., and Richardson, D. C. (2003) Structure validation by Cα geometry: ϕ, ψ and Cβ deviation, *Proteins: Struct., Funct., Genet. 50*, 437−450.

BI061517B